Breaking the regioselectivity rule for acrylate insertion in the Mizoroki–Heck reaction

Philipp Wucher[a], Lucia Caporaso[b,1], Philipp Roesle[a], Francesco Ragone[b], Luigi Cavallo[b], Stefan Mecking[a,1], and Inigo Göttker-Schnetmann[a,1]

[a]Department of Chemistry, University of Konstanz, 78464 Konstanz, Germany; and [b]Department of Chemistry, University of Salerno, Via Ponte Don Melillo, 84084 Fisciano, Salerno, Italy

In modern methods for the preparation of small molecules and polymers, the insertion of substrate carbon–carbon double bonds into metal–carbon bonds is a fundamental step of paramount importance. This issue is illustrated by Mizoroki–Heck coupling as the most prominent example in organic synthesis and also by catalytic insertion polymerization. For unsymmetric substrates $H_2C = CHX$ the regioselectivity of insertion is decisive for the nature of the product formed. Electron-deficient olefins insert selectively in a 2,1-fashion for electronic reasons. A means for controlling this regioselectivity is lacking to date. In a combined experimental and theoretical study, we now report that, by destabilizing the transition state of 2,1-insertion via steric interactions, the regioselectivity of methyl acrylate insertion into palladium–methyl and phenyl bonds can be inverted entirely to yield the opposite "regioirregular" products in stoichiometric reactions. Insights from these experiments will aid the rational design of complexes which enable a catalytic and regioirregular Mizoroki–Heck reaction of electron-deficient olefins.

density functional theory calculation | homogeneous catalysis | organometallic | regiochemistry

Whereas the palladium-catalyzed Mizoroki–Heck coupling is an established powerful strategy for the formation of carbon–carbon bonds from electron-deficient and electron-rich olefins (1–5), insertion (co)polymerization (6–8) of acceptor or donor substituted olefins has only been demonstrated since the mid-1990s, and only a few catalyst motifs are known to promote such polymerizations (9, 10), which are based on palladium. The regioselectivity of insertion follows the same pattern for both reactions. Electron-deficient olefins [e.g., methyl acrylate (MA)] selectively insert in a 2,1-fashion (6, 9–11), whereas electron-rich olefins (e.g., vinyl ethers) insert in a 1,2-fashion (3, 6, 12–14, †) (Fig. 1). Finally, apolar olefins (e.g., α-olefins) commonly afford mixtures of both insertion modes in palladium-catalyzed Mizoroki–Heck (15) and polymerization reactions (16), whereas closely related nickel-catalyzed polymerizations of α-olefins can proceed with high selectivity by 1,2-insertion (17)—e.g., under kinetically controlled low-temperature conditions when sterically demanding ligands coordinate to nickel (16, 18).

The accepted rationale for these reactivity patterns is that electronic effects govern the regiochemistry of insertion for polarized carbon–carbon double bond substrates: In the Cossée-Arlman-type insertion step, the metal-bound, nucleophilic carbon atom migrates to the lower electron-density carbon atom of the double bond, while the electrophilic palladium atom migrates to the higher electron-density carbon atom of the double bond. In contrast, the insertion regiochemistry of apolar carbon–carbon double bonds is rather determined by steric effects (given that there is little electronic discrimination of the two olefinic carbon atoms), and under strict kinetic control the 1,2-insertion mode may prevail. This intuitive rationale is supported by theoretical studies both of Mizoroki–Heck (19, 20) and polymerization catalysis (21, 22), which clearly indicate the predominance of electronic factors for the insertion of polarized olefins, particu-
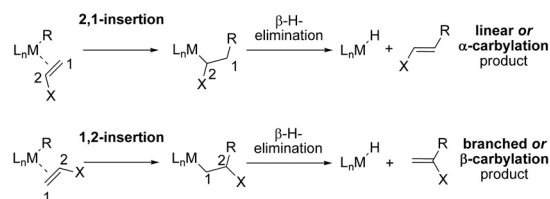

Fig. 1. Insertion modes of olefins into metal–carbon bonds and release of organic products by β-hydride elimination.

larly for electron-deficient olefins. Although the reliability of this concept to predict the regiochemistry of olefin insertions into metal–carbon bonds is impressive, for electron-deficient olefins it suggests a substantial limitation concerning product formation from opposite regiochemistry of insertion.

Recent studies of the catalytic properties of the [di(2-anisyl) phosphin-2-yl]benzenesulfonato Pd(II) methyl fragment (1) revealed that a weakly coordinated ligand such as DMSO in the single component catalyst precursor 1-DMSO enables the catalytic homooligomerization of MA by a selective 2,1-insertion mechanism (23). A similar high reactivity and selectivity toward MA was also observed after silver-mediated chloride abstraction from the sodium chloride coordinated complex 1-[Cl-Na(acetone)] to form the catalytically active fragment 1 (24) (Figs. 2, *Left* and 3, *Upper*). The latter system is beneficial for quantitative studies of insertion rates because, by comparison to 1-DMSO, the actual insertion step of interest is not overlayed by the DMSO dissociation preequilibrium.

In fragment 1, the anisyl groups of the (2-anisyl)$_2$P phosphine moiety are oriented away from the metal center, enforced by the tetrahedral environment of the phosphorus atom. In order to influence the insertion event of an olefin by increased steric interactions, substituents at the phosphorus atom must be forced into closer proximity to the metal. This aim was realized by incorporation of the phosphorus-donor into a rigid 1,3-diaza-2-phospholidine heterocycle substituted with bulky mesityl- or 2,6-di(isopropyl)phenyl groups. In [N,N′-di(aryl)-1,3-diaza-2-phospholidin-2-yl]benzenesulfonato palladium methyl complexes

Fig. 2. Phosphine sulfonato and diazaphospholidine sulfonato palladium(II) methyl complexes.

(2a,b-L) the *ortho*-substituents of the *N,N′*-arene rings are in close proximity to the palladium center (Fig. 2, *Right*; synthetic procedures and X-ray diffraction data can be found in the *SI Appendix* and Dataset S1). A more quantitative evaluation of the steric situation at the palladium center in fragments 2a and 2b (and for comparison, fragment 1) was obtained by theoretically calculated steric maps (see below).

Results and Discussion

The reaction of mesityl-substituted complexes 2a-DMSO and 2a-[Cl-Li(acetone)] (in the presence of silver triflate) as well as 2,6-(disopropyl)phenyl substituted complex 2b-[Cl-Li (tetrahydrofuran)$_2$] (in the presence of silver triflate) with excess MA (20 to 25 equivalents) in deuterated methylene chloride was monitored by proton (^{1}H) and phosphorus (^{31}P) NMR spectroscopy. As with complexes 1-L (23, 24), insertion of MA into the palladium-methyl bonds of fragments 2a and 2b takes place at 298 K. However, whereas MA insertion into fragment 1 proceeds selectively by 2,1-insertion, MA insertion into fragments 2a and 2b proceeds selectively by 1,2-insertion, as judged by formation of the insertion products 3a and 3b in *ca.* 95% NMR yield and *ca.* 85% isolated yield (Fig. 3, *Lower*). Under pseudo-first-order conditions (20 to 25 equivalents of MA), fragment 2a generated by silver-mediated and instantaneous chloride abstraction from 2a-[Cl-Li(acetone)] reacts by MA insertion with a rate constant $k_{obs} = 6.0(\pm0.1) \times 10^{-4}$ s^1 at 298 K, whereas the sterically more demanding species generated from 2b-[Cl-Li (tetrahydrofuran)$_2$] decays with $k_{obs} = 4.8(\pm0.1) \times 10^{-4}$ s^{-1} at an elevated temperature of 318 K. These rate constants compare to $k_{obs} = 12.4(\pm0.2) \times 10^{-4}$ s^{-1} at 298 K for the disappearance of fragment 1 (obtained by chloride abstraction from 1-[Cl-Na(acetone)]) in the presence of MA (25). From these data it seems obvious that steric interactions have a pronounced influence on the barrier of MA insertion.

The identity of 1,2-MA insertion products 3a and 3b is unambiguously established by one- and two-dimensional NMR techniques of the crude reaction mixtures (for details, see *SI Appendix*) by X-ray diffraction analyses of the isolated complexes after recrystallization (Fig. 4), by elemental analyses, and by quantitative formation of methyl methacrylate by β-hydride elimination upon NMR-monitored thermolysis of 3b.

In addition to the highly selective formation of complexes 3a, 3b by 1,2-MA insertion into 2a, 2b, reaction of 2a and 2b with
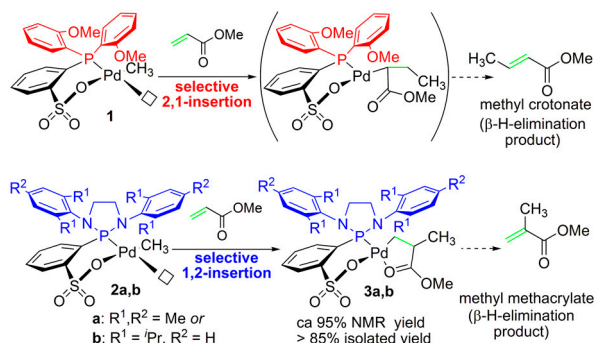
Fig. 3. (*Upper*) Selective 2,1-insertion of MA into fragment 1 (23, 24); (*Lower*) 1,2-insertion of MA into fragment 2 to form complexes 3a and 3b.
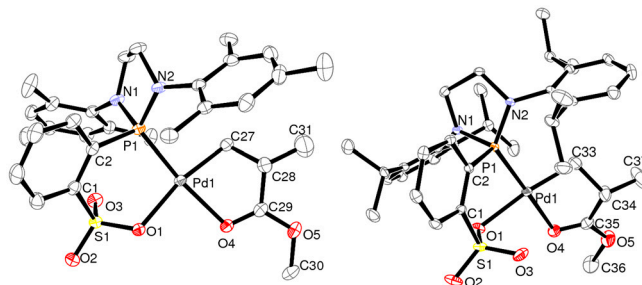
Fig. 4. Ortep plots of the 1,2-MA-insertion product 3a (*Left*) and 3b. Ellipsoids are shown with 50% probability. Hydrogen atoms are omitted for clarity.

MA forms trace amounts (<5% NMR yield) of methyl crotonate by 2,1-insertion of MA and concomitant β-hydride elimination (see *SI Appendix*).

Density functional theory calculations at the BP86 generalized gradient approximation level (26–28) illuminate the origin of the unusual regioselectivity of MA insertion with fragments 2a and 2b. As for fragment 1 (24), MA insertion into fragments 2a and 2b according to these calculations proceeds by η^2-coordination of MA *trans* to the phosphorus donor atom, followed by *cis-trans* isomerization to the less stable *cis* isomer from which insertion occurs (Fig. 5). However, whereas the rate-determining transition state for 2,1-insertion of MA into fragment 1 is favored by 10 kJ mol^{-1} over the 1,2-insertion transition state (Fig. 5, first line), 1,2-insertion of MA into fragment 2b is favored over 2,1-insertion by 9 kJ mol^{-1} (Fig. 5, second line). Consistent with calculations on fragment 2b, a preference for 1,2-insertion of MA is also calculated for fragment 2a (R = mesityl), although the difference is only 3 kJ mol^{-1} (see *SI Appendix*). Assuming similar entropic contributions for the insertion of MA into fragments 1, 2a, and 2b, the calculated energies are in qualitative agreement with the experimentally observed regiochemistry of insertion.

Inspection of the transition state geometries for MA insertion into fragment 2b (Fig. 6) reveals that the 2,6-di(isopropyl)phenyl groups of the [*N,N′*-di(aryl)-1,3-diaza-2-phospholidin-2-yl]benzenesulfonato ligands are in close proximity to the MA-methoxycarbonyl group in the transition state for the 2,1-insertion resulting in repulsive energetic contributions. To alleviate this steric clash in the transition state for 2,1-insertion into 2b, the MA rotates away from the nearby 2,6-di(isopropyl)phenyl group, resulting in a deviation from planarity of the four center Cossée-Arlman-like transition state (the Me-Pd-C2-C1 dihedral angle is −20°, see Fig. 6E; the respective dihedral angle is −27° for the 2,1-insertion transition state of 2a, see *SI Appendix*). In contrast, the [di(2-anisyl)phophin-2-yl]benzenesulfonato ligand of fragment 1 does not sterically interfere as severely with the coordinated MA in the 2,1-insertion transition state (Fig. 6B), which results in an almost perfectly planar geometry (the Me-Pd-C2-C1 dihedral angle is −4°, see Fig. 6B). In addition, inspection of the corresponding transition states for 1,2-insertion (Fig. 6 A and D) reveals that the coordinated MA does not sterically interfere with any of the phosphine sulfonato ligands of the precursor fragments 1 or 2b (and 2a, see *SI Appendix*). The absence of steric pressure in the 1,2-transition state allows the reacting atoms to assume an almost planar geometry both in 1 and 2b (the Me-Pd-C1-C2 dihedral angle is ~0°, see Fig. 6 A and D).

Steric maps (29, 30) based on calculated ground state geometries of 1-DMSO and 2b-DMSO show that all phosphine sulfonato ligands exert some steric pressure in the two bottom quadrants (Fig. 6 C and F) of the first coordination sphere around the palladium atom. In the event of a 2,1-insertion, the methoxycarbonyl group of MA will occupy one of these bottom quadrants in the insertion transition state, whereas in the event of
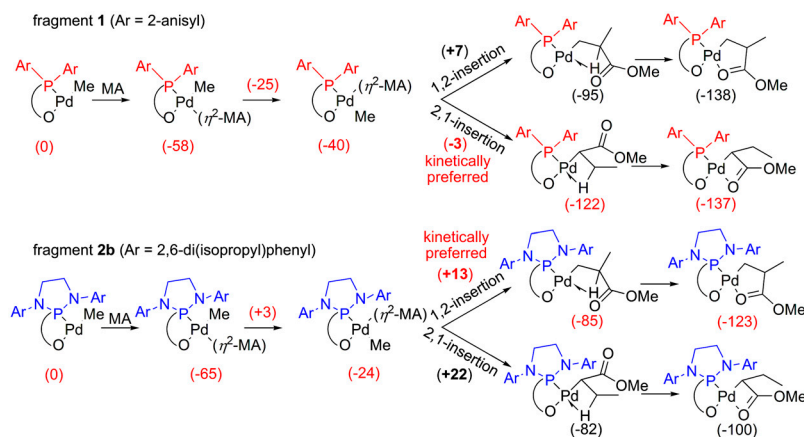
Fig. 5. Calculated 2,1- and 1,2-insertion of MA into the Pd-methyl (Pd-Me) bond of fragments 1 and 2b. Energies in kilojoule per mole. Transition state energies biasing 1,2- vs. 2,1-insertion are in bold.

a 1,2-insertion, one of the top quadrants will be occupied by the methoxycarbonyl group. Although the map of fragment 1 (Fig. 6C) displays some steric pressure in both bottom quadrants, the bottom-left quadrant is much less encumbered than the bottom-right quadrant, and the MA molecule inserts with the methoxycarbonyl group occupying the bottom-left quadrant which results in the electronically favored 2,1-insertion (Fig. 6 B and C). However, in fragment 2b (Fig. 6F) both bottom quadrants are highly encumbered, resulting in a destabilization of the transition state for the 2,1-insertion relative to that for the 1,2-insertion with the methoxycarbonyl group in the top-right quadrant (Fig. 6 C and F).

These experimental and theoretical data indicate that the strong preference of fragments 2a and 2b for the regioirregular 1,2-insertion of MA results from a severe destabilization of the (electronically favored) 2,1-insertion transition states by repulsive steric interactions of the incoming MA with the N,N'-di(aryl)-1,3-diaza-2-phospolidine moiety of the chelating ligand, which does not affect the 1,2-transition states to this extent.

The above systems most specifically resemble the active species of olefin insertion polymerization chemistry in that the Pd-methyl species represent the growing polymeryl chain. In the Mizoroki–Heck reaction, sp^2 carbon atoms are coupled to olefins. To this end, applicability of the concept of steric destabilization of the 2,1-insertion transition state to the decisive elementary step of the Mizoroki–Heck reaction of electron-deficient olefins was probed.

In a control experiment, the reaction of [di(2-anisyl)phosphin-2-yl]benzenesulfonato palladium phenyl (4-MeOH) with 25 equiv of MA in methylene chloride-d_2 solution was monitored by ^{1}H NMR spectroscopy. Insertion of MA into the palladium phenyl bond is complete within 30 min at 318 K, and, as expected, gives the regioregular Mizoroki–Heck product, methyl cinnamate (compound 5), by selective 2,1-insertion in nearly quantitative NMR yield (Fig. 7, first line).

In contrast, chloride abstraction from {N,N'-di[2,6-di(isopropyl)phenyl]-1,3-diaza-2-phospholidin-2-yl}benzenesulfonato palladium phenyl (6b-[Cl-Li·2(acetone/DMSO)]) by silver triflate in the presence of 25 equiv MA yields only ca. 7% methyl cinnamate (compound 5) under otherwise identical conditions, whereas the 1,2-insertion product 7b is formed in ca. 90% NMR yield. The thermal stability of 7b allowed isolation (83% yield) and full characterization by NMR techniques and elemental analysis. The identity of 7b was further corroborated by thermally induced β-hydride elimination in tetrachloroethane-d_2 solution (11 h at 363 K), which gave the regioirregular Mizoroki–Heck product (2-phenyl)MA (compound 8) in quantitative NMR yield (Fig. 7, second line). (For preparation procedures and characterization, see *SI Appendix*.)

In summary, these findings present a concept which allows reversal of the commonly valid regioselectivity rule for the insertion of the electron-deficient olefin MA into palladium carbon bonds. Appropriately arranged steric bulk of the ligands bound to the palladium center results in a severe steric repulsion with the incoming substrate in the electronically favored 2,1-insertion transition states. This steric repulsion makes the less sterically encumbered 1,2-insertion transition states competitive and strongly favored, thus overriding the usual distinct electronic determination of the insertion reaction. Although the regioirregular Mizoroki–Heck reaction of MA to form (2-phenyl)MA is so far stoichiometric in palladium, the concept of sterically destabilizing the electronically favored transition state of insertion elaborated in this work will certainly aid the rational design of catalysts that provide selective access to a catalytic regioirregular Mizoroki–Heck reaction.

Materials and Methods

Full experimental details and spectral data are included in the *SI Appendix*. Unless noted otherwise, all manipulations of phosphorous halides or palladium complexes were carried out under an inert nitrogen or argon atmosphere using standard glovebox or Schlenk techniques. Methylene
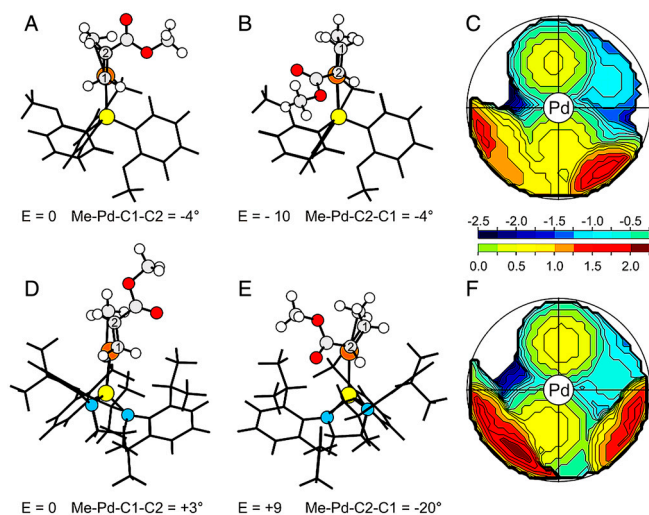
Fig. 6. Transition state geometries for 1,2- (*Left*) and 2,1-insertion (*Center*) of MA into the Pd-Me bond of fragment 1 (*A* and *B*) and of fragment 2b (*D* and *E*). Relative energies (E) in kilojoule per mole. Steric maps (*Right*) of the fragments 1 (*C*) and 2b (*F*). The colored scale indicates the isocontour levels, in angstrom. Orientation of the ligands in the steric maps as in *A* and *B* and *D* and *E*.
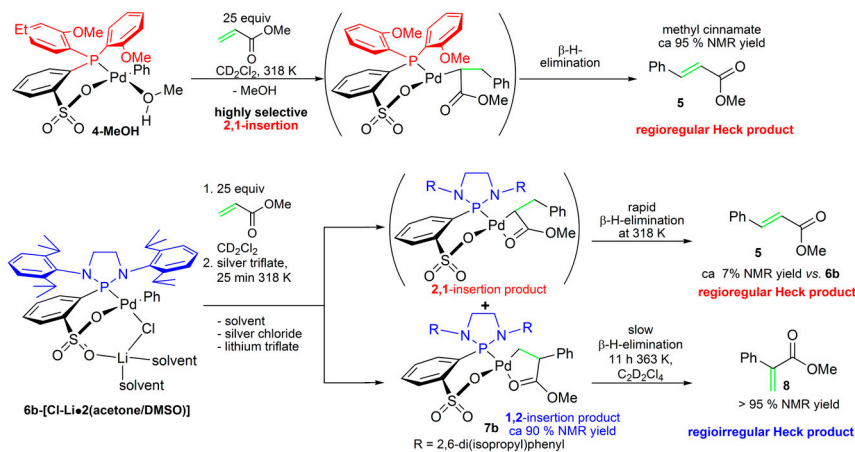
Fig. 7. Regioregular 2,1-insertion of MA into complex 4-MeOH (first line) and selective regioirregular 1,2-insertion of MA into complex 6b-[Cl-Li•2(acetone/DMSO)] (second line).

chloride, DMSO, and pentane were distilled from calcium hydride, toluene and benzene from sodium, THF and diethyl ether from blue sodium/benzophenone ketyl, and methanol from activated (iodine) magnesium under argon prior to use. Acetone per analysis and MA were degassed by repetitive freeze–thaw cycles and used without further purification. All other solvents were commercial grade. Palladium(II)-chloride was obtained from Merck, 2,4,6-trimethylaniline (98%) and 2,6-di(isopropyl)aniline (90%, technical grade) was purchased from Acros, and trichlorophosphine (99%) was purchased from Riedel-de Haën. Cyclooctadiene palladium-methyl chloride (31) and 2-chloro-1,3-di(aryl)-1,3,2-diazaphospholidines (32) were synthesized according to literature procedures. All deuterated solvents were supplied by Eurisotop. The identity of so-far unreported compounds was established by 2D NMR experiments [^{1}H-^{1}H gCOSY, ^{1}H-^{13}C gradient heteronuclear single quantum coherence (gHSQC), and ^{1}H-^{13}C gradient heteronuclear multiple bond correlation (gHMBC)] in addition to 1D NMR experiments. NMR temperature calibration was performed using pure methanol (low-temperature) or ethylene glycol (high-temperature) samples. NMR spectra were recorded on a Varian Unity Inova 400, a Bruker Avance III DRX 400, or a Bruker Avance DRX 600 instrument. ^{1}H NMR spectra were referenced to residual protiated solvent signals. ^{13}C NMR spectra were referenced to the solvent signals, and ^{31}P NMR spectra to external 85% H$_3$PO$_4$. The purity of so-far unreported compounds was established by elemental analyses. Single crystals of complexes 2a-DMSO, 2a-LiCl•(MeOH), 2b-LiCl•(2 THF), 3a, 3b, 4-MeOH•(MeOH), and 6b-LiCl•(acetone/DMSO) were analyzed by X-ray diffraction analysis.

Computational Details. The Amsterdam Density Functional (ADF) program (26, 33–35) was used. The electronic configuration of the molecular systems was described by a triple-ζ Slater-type orbitals (STO) basis set on Pd (ADF basis set TZV). Double-ζ STO basis sets, augmented by one polarization function, were used for main group atoms (ADF basis sets DZVP). The inner shells on Pd (including 3d), P and S (including 2p) C and O (1s), were treated within the frozen core approximation. Energies and geometries were evaluated using the local exchange-correlation potential of Vosko et al. (35), augmented in a self-consistent manner with Becke's (26) exchange gradient correction and Perdew's (27, 28) correlation gradient correction (BP86 functional). The transition states were approached through a linear transit procedure starting from the coordination intermediates. The forming C–C bond was assumed as reaction coordinate during the linear transit scans. Full transition state searches were started from the maxima along the linear transit paths. Steric maps were constructed as indicated in the *SI Appendix*.

Exemplified procedure for the preparation of {[(κ²-P,O)-2-(1,3-di(2,6-diisopropyl)phenyl-1,3,2-diazaphospholidin-2-yl) benzenesulfonato] palladium(II)-[(κ²-C,O)-3-methoxy-2-phenyl-3-oxopropyl]} (7b). *Lithium 2-[1,3-di(2,6-diisiopropyl)phenyl-1,3,2-diazaphospholidin-2-yl) benzenesulfonate (L1b).* To a solution of benzenesulfonic acid (1582 mg, 10 mmol) in THF (35 mL) in a septum capped Schlenk tube was slowly added by syringe butyl lithium (14 mL 1.6 M pentane solution, 22.4 mmol) at 298 K under stirring. The formed suspension was stirred for 30 min at 298 K, then cannula transferred into a Schlenk frit, and filtrated. After washing with pentane (4 × 15 mL) the off-white powder was dried under high vacuum (10⁻³ mbar) to leave o-dilithiobenzenesulfo-

nate•(0.75 THF) (2180 mg, 9.60 mmol, 96%) which was used in the next step without further purification.

To o-dilithiobenzenesulfonate•(0.75 THF) (448 mg, 2 mmol) and 2-chloro-1,3-[di-(2,6-diisopropyl)phenyl]-1,3,2-diazaphospholidine (935 mg, 2.1 mmol) in a 20-mL Schenk tube was added THF (10 mL) and the resulting suspension was heated under stirring to 340 K for 1 h. The clear solution was cooled to room temperature and the solvent removed in vacuo (10⁻³ mbar). Diethyl ether (10 mL) was added to the remaining glassy solid and the mixture was sonicated for 20 min while a fine white precipitate formed. The white precipitate was cannula transferred into a Schlenk frit, washed with diethyl ether (2 × 5 mL) and pentane (2 × 10 mL), dried under high vacuum, and dissolved in hot benzene (50 mL). The resulting opaque mixture was filtrated through a pad of celite, and the solvent removed in vacuo. The remaining solid was triturated with pentane (10 mL) to yield ligand L1b containing 1 equiv of diethyl ether (1072 mg, 1.66 mmol, 82.8%) after drying under vacuum.

[(DMSO)₂Pd(Ph)Cl]. In a 100-mL Schlenk tube, palladium dichloride (887 mg, 5 mmol) was dissolved in DMSO (6 mL) at 383 K under stirring. After cooling to 298 K, diethyl ether was added (70 mL) under stirring, the resulting orange solid collected by filtration, washed with diethyl ether (4 × 10 mL), and dried under vacuum to yield [(DMSO)₂PdCl₂] (1.630 g, 4.89 mmol, 97.7%). To a suspension of [(DMSO)₂PdCl₂] (334 g, 1 mmol) in a mixture of DMSO (3 mL) and THF (15 mL) in a 50 mL septum capped Schlenk tube was added tetraphenyl tin (215 mg, 503.3 μmol). The solution was stirred for 8 h at 298 K while the orange starting material dissolved and an orange-red solution containing some palladium black formed. The mixture was concentrated to ca. 5 mL, DMSO (5 mL) was added and the resulting mixture filtered through a syringe filter into a 100-mL Schlenk flask. Removal of all volatiles under high vacuum (298 K, 10⁻³ mbar) gave an orange solid, which was dispersed in THF (15 mL) and cannula transferred into a Schlenk frit. The solid was filtered off, washed with THF (4 × 10 mL), and dried under vacuum to yield [(DMSO)₂Pd(Ph)Cl] which contained traces of palladium black (361.1 mg, 0.965 mmol, 96.5%).

{(κ²-P,O)-2-[1,3-di(2,6-diisopropyl)phenyl-1,3,2-diazaphospholidin-2-yl] benzenesulfonato]-palladium(II)-phenyl} lithium chloride adduct [6b-LiCl•(DMSO)]. To L1b • (Et₂O) (65 mg, 100 μmol) and [(DMSO)₂Pd(Ph)Cl] (previous step; 39.8 mg, 106 μmol) in an NMR tube was added methylene chloride-d₂ (400 μL). The tube was shaken for 5 min at 298 K and then centrifuged. Monitoring of the solution by ^{1}H and ^{31}P NMR indicated consumption of L1b • (Et₂O) and formation of one new ^{31}P containing species in >90% NMR yield. The solution was filtrated, concentrated to dryness, and the resulting solid extracted with pentane (2 × 3 mL) to yield complex 6b-LiCl•(DMSO) after drying under vacuum (66.7 mg, 72 μmol, 72%). Crystals of 6b-LiCl• (1.8 acetone, 0.2 DMSO) suitable for X-ray diffraction analysis were grown from 6b-LiCl•(DMSO) (12 mg) in acetone (60 μL) after layering with pentane.

{[(κ²-P,O)-2-(1,3-di(2,6-diisopropyl)phenyl-1,3,2-diazaphospholidin-2-yl] benzenesulfonato] palladium(II)-[(κ²-C,O)-3-methoxy-2-phenyl-3-oxopropyl]} (7b). To a solution complex 6b-LiCl•(DMSO) (38 mg, 41 μmol) in methylene chloride-d₂ in an NMR tube was added MA (88 mg, 1.03 mmol, 25 equiv). The

mixture was monitored by ^{1}H and ^{31}P NMR, then silver triflate (10.8 mg, 42 μmol, 1.02 equiv) was added and the tube was shaken for 2 min and centrifuged whereby silver chloride deposited. The resulting solution was monitored by ^{1}H and ^{31}P NMR at 318 K. Formation of complex 7b (ca. 90% NMR yield by ^{1}H and ^{31}P NMR) together with methyl cinnamate (5) (ca. 7% NMR yield) was complete after ca. 25 min at 318 K. Isolation of complex 7b was accomplished by filtration, removing all volatiles under vacuum, washing the residue with pentane (4 × 2 mL), and cold diethyl ether (1 mL, 243 K), and crystallization from methylene chloride (100 μL) after layering with pentane (1.5 mL) in an NMR tube (28.3 mg, 33.9 μmol, 82.6%).

Further procedures and data (synthetical procedures, analytical characterization of compounds, X-ray diffraction analyses data including a multiple cif-file, NMR spectra of key-compounds and in situ reactions, theoretical procedures, and calculated geometries and energies) are given in the *SI Appendix*.

1. Larhed M, Hallberg A (2002) *Handbook of Organopalladium Chemistry for Organic Synthesis*, ed E Negishi (Wiley, New York), pp 1133–1178.
2. Beller M, Zapf A, Riermeier TH (2004) *Transition Metals for Organic Synthesis*, eds M Beller and C Bolm (Wiley, Weinheim), pp 271–305.
3. Beletskaya IP, Cheprakov AV (2000) The Heck reaction as sharpening stone of palladium catalysis. *Chem Rev* 100:3009–3066.
4. Mizoroki T, Mori K, Ozaki A (1971) Arylation of olefin with aryl iodide catalyzed by palladium. *Bull Chem Soc Jpn* 44:581.
5. Heck RF (1968) Arylation, methylation and carboxyalkylation of olefins by group VIII metal derivatives. *J Am Chem Soc* 90:5518–5526.
6. Nakamura A, Ito S, Nozaki K (2009) Coordination—insertion copolymerization of fundamental polar monomers. *Chem Rev* 109:5215–5244.
7. Arlman EJ, Cossée P (1964) Ziegler-Natta catalysis. III. Stereospecific polymerization of propene with the catalyst system TiCl$_3$-AlEt$_3$. *J Catal* 3:99–104.
8. Cossée P (1960) On the reaction mechanism of the ethylene polymerization with heterogeneous Ziegler-Natta catalysts. *Tetrahedron Lett* 1(38):12–16.
9. Mecking S, Johnson LK, Wang L, Brookhart M (1998) Mechanistic studies of the palladium-catalyzed copolymerization of ethylene and α-olefins with methyl acrylate. *J Am Chem Soc* 120:888–899.
10. Drent E, van Dijk R, van Ginkel R, van Oort B, Pugh RI (2002) Palladium catalysed copolymerisation of ethene with alkylacrylates: Polar comonomer built into the linear chain. *Chem Commun* 744–745.
11. Kochi T, Noda S, Yoshimura K, Nozaki K (2007) Formation of linear copolymers of ethylene and acrylonitrile catalyzed by phosphine sulfonate palladium complexes. *J Am Chem Soc* 129:8948–8949.
12. Luo S, Jordan RF (2006) Copolymerization of silyl vinyl ethers with olefins by (α-diimine)PdR$^+$. *J Am Chem Soc* 128:12072–12073.
13. Luo S, Vela J, Lief GR, Jordan RF (2007) Copolymerization of ethylene and alkyl vinyl ethers by a (phosphinesulfonate)PdMe catalyst. *J Am Chem Soc* 129:8946–8947.
14. Cabri W, Candiani I (1995) Recent developments and new perspectives in the Heck reaction. *Acc Chem Res* 28:2–7.
15. Fall Y, Berthiol F, Doucet H, Santelli M (2007) Palladium-tetraphosphine catalysed Heck reaction with simple alkenes: Influence of reaction conditions on the migration of the double bond. *Synthesis* 11:1683–1696.
16. McCord EF, et al. (2007) ^{13}C NMR analysis of α-olefin enchainment in poly(α-olefins) produced with nickel and palladium α-diimine catalysts. *Macromolecules* 40:410–420.
17. Möhring VM, Fink G (1985) Novel polymerization of α-olefins with the catalyst system nickel/aminobis(imino)phosphorane. *Angew Chem Int Ed Engl* 24:1001–1003.
18. Rose JM, Cherian AE, Coates GW (2006) Living polymerization of α-olefins with an α-diimine Ni(II) catalyst: Formation of well-defined ethylene-propylene copolymers through controlled chain-walking. *J Am Chem Soc* 128:4186–4187.
19. von Schenck H, Åkermark B, Svensson M (2003) Electronic control of the regiochemistry in the Heck reaction. *J Am Chem Soc* 125:3503–3508.
20. Deeth RJ, Smith A, Brown JMJ (2004) Electronic control of the regiochemistry in palladium-phosphine catalyzed intermolecular Heck reactions. *J Am Chem Soc* 126:7144–7151.
21. Philipp DM, Muller RP, Goddard WA, McAdon M, Mullin M (2002) Computational insights on the challenge for polymerizing polar monomers. *J Am Chem Soc* 124:10198–10210.
22. Michalak A, Ziegler T (2001) DFT studies on the copolymerization of α-olefins with polar monomers: Ethylene-methyl acrylate copolymerization catalyzed by a Pd-based diimine catalyst. *J Am Chem Soc* 123:12266–12278.
23. Guironnet D, Roesle P, Rünzi T, Göttker-Schnetmann I, Mecking S (2009) Insertion polymerization of acrylate. *J Am Chem Soc* 131:422–423.
24. Guironnet D, et al. (2010) Mechanistic insights on acrylate insertion polymerization. *J Am Chem Soc* 132:4418–4426.
25. Rünzi T, Guironnet D, Göttker-Schnetmann I, Mecking S (2010) Reactivity of methacrylates in insertion polymerization. *J Am Chem Soc* 132:16623–16630.
26. Becke AD (1988) Density-functional exchange-energy approximation with correct asymptotic behavior. *Phys Rev A* 38:3098–3100.
27. Perdew JP (1986) Density-functional approximation for the correlation energy of the inhomogeneous electron gas. *Phys Rev B Condens Matter Mater Phys* 33:8822–8824.
28. Perdew JP (1986) Erratum: Density-functional approximation for the correlation energy of the inhomogeneous electron gas. *Phys Rev B Condens Matter Mater Phys* 34:7406.
29. Ragone F, Poater A, Cavallo L (2010) Flexibility of N-heterocyclic carbene ligands in ruthenium complexes relevant to olefin metathesis and their impact in the first coordination sphere of the metal. *J Am Chem Soc* 132:4249–4258.
30. Poater A, Ragone F, Mariz R, Dorta R, Cavallo L (2010) Comparing the enantioselective power of steric and electrostatic effects in transition metals catalyzed asymmetric synthesis. *Chem Eur J* 16:14348–14353.
31. Rulke RE, et al. (1993) NMR study on the coordination behavior of dissymmetric terdentate trinitrogen ligands on methylpalladium(II) compounds. *Inorg Chem* 32:5769–5778.
32. Abrams MB, Scott BL, Baker RT (2000) Sterically tunable phosphenium cations: Synthesis and characterization of bis(arylamino)phosphenium ions, phosphinophosphenium adducts, and the first well-defined rhodium phosphenium complexes. *Organometallics* 19:4944–4956.
33. Vrije Universiteit (2007) *ADF2007, Theoretical Chemistry, Users's Manual* (Vrije Universiteit, Amsterdam).
34. Baerends EJ, Ellis DE, Ros P (1973) Self-consistent molecular Hartree-Fock-Slater calculations I. The computational procedure. *Chem Phys* 2:41–51.
35. Vosko SH, Wilk L, Nusair M (1980) Accurate spin-dependent electron liquid correlation energies for local spin density calculations: A critical analysis. *Can J Phys* 58:1200–1211.

CHEMISTRY